Indian Journal of Pure & Applied Physics
Vol. 61, September 2023, pp. 739-743
DOI: 10.56042/ijpap.v61i9.3209

A Two-step Method to Grow ZnSe Thin Films and To Study their Characteristics

Zakir Hussain, Naresh Padha*, Shafiq Ahmad & Padma Dolma

Department of Physics, University of Jammu, Jammu 180 006, India

Received 28 June 2023; accepted 7 August 2023

The ZnSe material synthesised by the fusion method was used to deposit 200 nm thin layers on corning glass substrate at 300 K in a vacuum ($2x10^{-6}$ mbar). The as-deposited films were annealed at 573 K in a vacuum ($1x10^{-3}$ mbar). The obtained crystallites provide the most significant peak (MSP) along (111) orientations corresponding to a zinc blende structure. Further, the grown samples show maximum transmittance of ~ 90% in visible - NIR regions of the E M Spectrum. The layers possess the direct bandgap (E_g) of 2.02 (300 K) and 2.57 eV (573 K). The surface morphology indicates the uniform spread of nanocrystalline particles over the substrate. Thus, the obtained ZnSe films are useful as buffer/window layers in solar cell structures.

Keywords: ZnSe; Thin films; Solar Cells; Transmittance

1 Introduction

In developing CdTe/CIGS-based photovoltaic solar cells, cadmium sulphide (CdS) is frequently used as a buffer/window layer to transmit maximum incident light to the absorber layer[1]. But, CdS has limitations; it is hazardous to the environment due to the toxic nature of Cd. Thus, there is a need to develop a Cd-free alternate material for window or buffer layer. Zn-based semiconducting materials such as ZnSe, ZnS, and ZnO are substitutes for CdS in thin film solar cell technology[2]. Among these, ZnSe is a promising material with a direct wide bandgap of 2.7 eV with high optical transparency of ~ 90%[3]. It crystallises into two structural forms: cubic and hexagonal[4]. ZnSe is environmentally friendly and allows more incident light to the corresponding absorber layer. As a result, present thin film technology encourages the usage of ZnSe as a suitable buffer/window layer material[5]. Several deposition techniques have been used to grow ZnSe thin films, Viz. electron beam evaporation, chemical bath deposition, RF sputtering, Sol-gel method *etc.*[6]. In the present research, a two-step method was used for synthesising ZnSe material and the growth of its thin films. The grown layers were undertaken for the structural, optical, and morphological characteristics.

*Corresponding author:
(E-mail: nareshpadha@gmail.com;
nareshpadha@jammuuniversity.ac.in)

2 Materials and Methods

A two-step method was used to grow the thin films of ZnSe. Step one involves mixing 99.999% pure Zn shots and Se powder stoichiometrically in a 1:1 atomic ratio, followed by fusion at high temperatures. The precursors were sealed at a base pressure of ~ $1x10^{-6}$ mbar using a vacuum tube sealing unit VS-150D (HHV, India). The sealed ampoule was heated to 1100 ºC at 4 ºC /minute in a microprocessor PID-controlled furnace MT-11 (METREX) and kept at this temperature for six hours. It was cooled to room temperature at the same rate, forming a ZnSe ingot. The ingot was crushed into powder to an average particle size of ~ 100 nm. Secondly, the ZnSe thin films of 200 nm were deposited on corning glass substrate at 300 K under vacuum $1x10^{-6}$ mbar in a vacuum coating unit 12A4DM (HHV, India). The thickness of the depositing films was measured using a digital thickness monitor DTM-101(HHV, India). The deposited films were annealed at 573 K for 40 minutes in a tubular furnace under a vacuum of ~ $1x10^{-3}$ mbar. The structural analysis of the films was performed by using the powder X-ray diffractometer X'pert[3] (PANalytical) fitted with HD bragg brentano incident geometry in the 2θ range 10° – 70° in line scan mode with a scan speed of 0.03°/s using Ni filtered $CuK\alpha_1$ (λ;1.5406A°). The surface morphology of the samples was determined using a field emission scanning electron microscope (FESEM) Gemini 500 (Carl Zeiss) at an accelerating voltage of 20 KV. The

compositional analysis of the samples was carried out by energy dispersive X-ray analysis (EDAX) using the octane elect EDS system (Ametek). The optical data were collected using reflectometer FR-portable (Theta Metrisis).

3 Results and Discussion

3.1 Structural Analysis

The X-ray diffraction (XRD) patterns of ZnSe films as-deposited at 300 K and grown on annealing at 573 K are shown in Fig. 1.

The XRD patterns exhibit a high-intensity peak along (111) oriented planes and a broad (220) peak at 2θ values of 45.63º. These peaks correspond to the ZnSe zincblende structure (cubic phase) as determined based on JCPDS card no. 37-1463. Further, the intensity of the (111) peak increases on annealing at 573 K; similar ZnSe behaviour has also been reported earlier[7]. The enhancement in the intensity and crystallite size indicates an improvement in the crystallinity of the deposited films. However, the 2θ value of the (111) peak is almost unchanged.

The average crystallite size (D) and interplanar spacing (d) corresponding to (111) peak were calculated using scherrer's formula and bragg's law mentioned in relations represented by Eqs. (1) & (2)[8]:

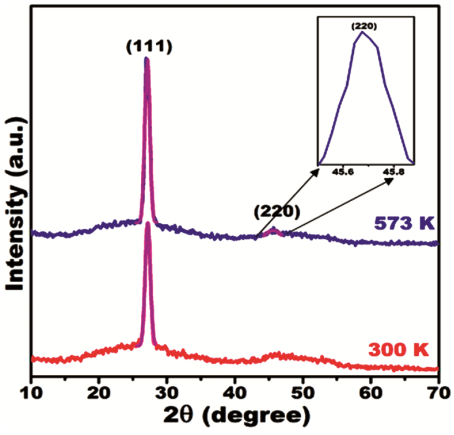

Fig. 1 — The X-ray diffraction patterns of the ZnSe films as-deposited at 300 K and grown on annealing at 573 K; the inserted figure shows the magnified view of the peak at 2θ of 45.63º.

$$D = \frac{0.94\lambda}{\beta cos\theta} \quad \ldots (1)$$

$$d = \frac{\lambda}{2sin\theta} \quad \ldots (2)$$

The crystallite size (D) was calculated using the gaussian fit of the diffracted peak; the results are shown in Table 1. The crystallite size of the (111) peak increases marginally from 10.48 (300 K) to 10.76 nm (573 K). The lattice constant of the cubic structure of ZnSe planes was calculated by using the relation (3) given below[9]:

$$\frac{1}{d^2} = \frac{(h^2+k^2+l^2)}{a^2} \quad \ldots (3)$$

Where 'd' is the interplanar spacing, (hkl) are miller indices, and 'a' represents the unit cell parameter. The intensity and average crystallite size of the (111) peak of the films as-deposited at 300 K and grown on annealing at 573 K exhibit minor changes. Table 1 presents structural parameters with slight variations between the as-deposited and 573 K annealed samples.

3.2 Optical Analysis

The transmittance percentage (T%) for the as-deposited and annealed samples as a function of wavelength (λ) is shown in Fig. 2(a). The transmittance of the as-deposited film was ~ 50%, whereas that of the films grown on annealing at 573 K increased to 90%. The annealed samples display higher T% in the visible-NIR region, which could be attributed to improved crystallinity in the films[10]. Besides, it is found that the transmission spectra of both films exhibit interference patterns beyond absorption edge, which reflect thickness homogeneity and good surface quality[10].

The absorption coefficient (α) was calculated from the T% using the relation given in Eq. (4)[15]:

$$\alpha = \frac{1}{t} \ln\left(\frac{100}{T\%}\right) \quad \ldots (4)$$

Where α is the absorption coefficient, T% is the transmission percentage, and t is film thickness.

Table 1 — The crystallite size, peak position, d-spacing and lattice parameter of (111) peak of the ZnSe films as-deposited at 300 K and grown on annealing at 573 K.

Sample Name	d (A°)	2θ (deg.)	Intensity (cps)	Cell Parameter (Å)	Crystallite size D (nm)	Vol. (Å^3)
As-deposited (300 K)	3.27	27.19	268	5.67	10.48	182.67
Annealed (573 K)	3.28	27.12	358	5.68	10.76	183.92

ZnSe: JCPDS (37-1463): Sys: Cubic (Face centered); Cell parameters: a = 5.668 Å; V = 182.09 Å^3

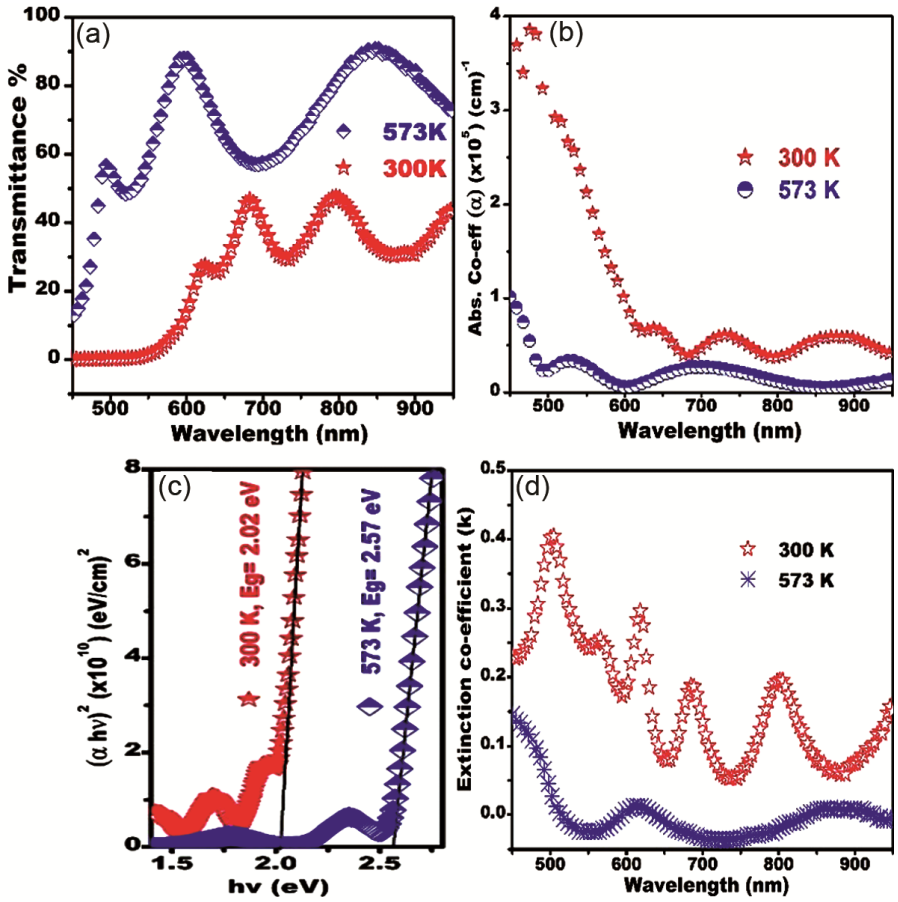

Fig. 2 — (a),(b) Transmission percentage (%) and absorption coefficient (α) versus wavelength (λ), (c) $(\alpha h\nu)^2$ as a function of photon energy (hν), and (d) extinction coefficient (K) versus wavelength (λ) of the films as deposited at 300 K and grown on annealing at 573 K.

The 'α' values decrease at 573 K, as shown in Fig. 2(b). It was also observed that the absorption edge of the annealed layer shifts towards a lower wavelength (blue shift), indicating an increase in the optical bandgap[6,11]. The as-deposited and annealed films show an absorption coefficient (α) ~ $1x10^5$ cm^{-1}. As reported by several authors, the sharp decrease in 'α' at shorter wavelengths in the annealed samples results from the direct allowed transition between the conduction band and ionised donor[2].

The optical bandgap (E_g) was calculated using Tauc's relation, which governed the relation between absorption coefficient (α) and photon energy (hν) as given in the mathematical relation mentioned in Eq. (5)[12]:

$$(\alpha h\nu)^n = A(h\nu - E_g) \quad \ldots (5)$$

Where A is a constant, hν is the photon energy, n=2 represents the direct allowed bandgap, and n=1/2 is the indirect allowed bandgap. The direct bandgap (E_g) value is 2.02 and 2.57 eV for as-deposited and annealed films, respectively {Fig. 3(c)}. Moreover, the E_g shifts towards shorter wavelengths (λ) at 573 K. The variation in E_g with annealing might be due to the change in stoichiometry and the crystallographic changes[13]. Another reason for the increase in Eg with annealing temperature may be the creation of localised states in the high photon energy region[14].

The extinction coefficient (κ) can be used to calculate the degree of surface uniformity and smoothness[15]. It was determined using the relation given in Eq. (6)[16]:

$$K = \frac{\alpha\lambda}{4\pi} \quad \ldots (6)$$

Where λ represents the wavelength of incident radiation, Fig. 2(d) represents the variation of κ value of samples as a function of wavelength (λ). The annealed films exhibit a value of κ less than 0.15 in the wavelengths from 450 to 950 nm (visible-NIR

Table 2 — Composition analysis of ZnSe thin films deposited at 300 K and grown on T_A ~ 573 K.

Sample Name	Weight %		Atomic %		Zn/Se (Atomic %)	Stoichiometry
	Zn	Se	Zn	Se		
As-deposited (300 K)	20.7	79.3	24.0	76.0	0.31	$ZnSe_{3.17}$
Annealed (573 K)	37.0	63.0	41.5	58.5	0.70	$ZnSe_{1.40}$

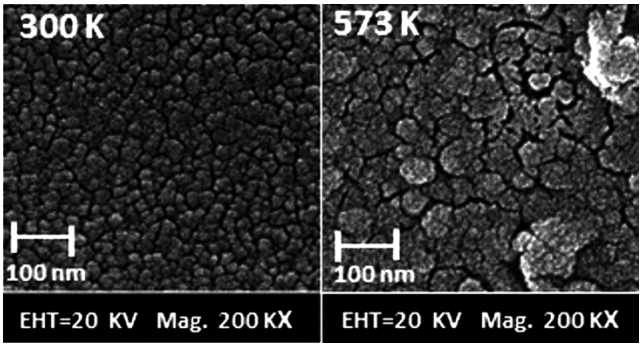

Fig. 3 — Surface morphological images of the thin films of ZnSe as-deposited at 300 K and grown on annealing at 573 K.

region), confirming the good surface quality of the annealed samples[17]. Thus, the optical response indicates that the undertaken films are useful for photovoltaic, optoelectronic devices and window/ buffer layers in solar cell structures.

3.3 Morphological and Compositional Analysis

The surface morphological graphs of the as-deposited and annealed films are presented in Fig. 3. The surfaces of the films are observed to be uniformly distributed across the substrate. The as-deposited film exhibits irregularly shaped grains distributed over the entire surface. However, in the sample grown at 573 K, the smaller particles are seen agglomerated into clusters of different shapes[18]. Some voids are also seen in the grown samples. The crystallite size increases from 26 (300 K) to 42 nm (573 K) on annealing at 573 K. Table 2 shows the compositional analysis results of the samples. The atomic percentage of Zn increases while that of Se decreases at 573 K. Therefore, the composition in the annealed samples is better than the as-grown films in stoichiometry, and it also provides better crystallinity. The decrease of the 'Se' percentage at 573 K compared to as-deposited samples is due to difference in the thermal coefficients between the corning glass substrate and the materials at T_A ~ 573 K[17].

4 Conclusion

ZnSe powder material was synthesised from the precursors using the fusion method at high temperatures. Thin films of this material were as-deposited at room temperature (300 K) and grown on annealing at 573 K. The grown layers of ZnSe show stability in the structure along (111) orientations. The optical properties of the films are sensitive to the annealing temperature (T_A). The transmittance spectra in the visible-NIR exhibit direct allowed bandgap (E_g) values of 2.02 (300 K), 2.57 eV (573 K), and absorption coefficient (α) > $1x10^5$ cm^{-1}. The films grown at 573 K exhibit better stoichiometry, crystallinity and smoother surface. These characteristics make the annealed films suitable as window/buffer layers in the solar cell structure and in various photonic devices.

Acknowledgement

One of the authors, Zakir Hussain, is grateful to the Council of Scientific and Industrial Research (CSIR)

Govt. of India for providing a senior research fellowship. The authors also thank the Ministry of Education, Govt. of India, for RUSA 2.0 grants. In addition, the authors are grateful to the Department of Science & Technology, the Government of India providing funding for the X-ray diffractometer under the PURSE & FIST programs.

References

1 Chander S & Dhaka M S, *Sol Energy* 150 (2017) 577.
2 Purohit A, Chander S, Sharma A, Nehra S P & Dhaka M S, *Opt Mater*, 49 (2015) 51.
3 Khan T M, Mehmood M F, Mahmood A, Shah A, Raza Q, Iqbal A & Aziz U, *Thin Solid Films*, 519 (2011) 5971.
4 Deng Z, Qi J, Zhang Y, Liao Q & Huang Y, *Nanotechnology*, 18 (2007) 475603.
5 Sharma J & Tripathi S K, *Physica B*, 406 (2011) 1757.
6 Chuhadiya S, Sharma R, Himanshu, Patel S L, Chander S, Kannan M D & Dhaka M S, *Physica E*, 117 (2019) 113845.
7 Suthar D, Chasta G, Himanshu, Patel S L, Chander S, Kannan M D & Dhaka M S, *Mater Res Bull*, 132 (2020) 110982.
8 Chasta G, Himanshu, Patel S L, Chander S, Kannan M D & Dhaka M S, *J Mater Sci: Mater Electron*, 33 (2022) 139.
9 Singh P, Singh S K, Singh P, Prakash R & Rai S B, *Mater Res Bull*, 122 (2020) 110663.
10 Rusu G I, Diciu M, Pirghie C & Popa E M, *Appl Surf Sci*, 253 (2007) 9500.
11 Bashar M S, Matin R, Sultana M, Siddika A, Rahaman M, Gafur M A & Ahmed F, *J Theoret Appl Phys*, 14 (2020) 53.
12 Hendia T A & Soliman L I, *Thin Solid Films*, 261 (1995) 322.

13 Dahiya A, Chuhadiy S, Himanshu, Suthar D, Nehra S P & Dhaka M S, *J Mater Sci: Mater Electron*, 34 (2023) 410.
14 Padha N & Kumar S, *Appl Phys A*, 127 (2021) 877.
15 Niranjan R & Padha N, *Mater Chem Phys*, 257 (2021) 123823.
16 Beena D & Lethy K J, *Appl Surf Sci*, 255 (2009) 8334.
17 Sharma T P & Sharma S K, *Indian J Pure Appl Phys*, 28 (1990) 486.
18 Kumar S, Banotra A, Padha N & Ahmed S, *Opt Mater*, 134 (2022) 113078.